Analysis of Folding and Unfolding Reactions of Cytochrome b_5[†]

Susan Manyusa, Gulnahar Mortuza, and David Whitford*

Structural Biochemistry, Molecular & Cellular Biology, Queen Mary & Westfield College, London E1 4NS, England

Received June 21, 1999; Revised Manuscript Received August 23, 1999

ABSTRACT: The guanidine hydrochloride- (GuHCl-) induced unfolding and refolding of a recombinant domain of bovine microsomal cytochrome b_5 containing the first 104 amino acid residues has been characterized by both transient and equilibrium spectrophotometric methods. The soluble domain is reversibly unfolded and the equilibrium reaction may be monitored by changes in absorbance and fluorescence that accompany denaturation of the native protein. Both probes reveal a single cooperative transition with a midpoint at 3 M GuHCl and lead to a value for the protein stability (ΔG_{uw}) of 26.5 kJ mol^{-1}. This stability is much higher than that reported for the corresponding form of the apoprotein (∼7 kJ mol^{-1}). Transient changes in fluorescence and absorbance during protein unfolding exhibit biphasic profiles. A fast phase occupying ∼30% of the total amplitude is observed at high denaturant concentrations and becomes the dominant process within the transition region. The rates associated with each process show a linear dependency on GuHCl concentration, and at zero denaturant concentration the unfolding rates (k_{uw}) are 4.5×10^{-5} s^{-1} and 5.2×10^{-6} s^{-1} at 25 °C. The pattern of unfolding is not correlated with covalent heterogeneity, since a wide range of variants and site-directed mutants exhibit identical profiles, nor is the unfolding correlated with cis−trans Pro isomerization in the native state. In comparison with the apo form of cytochrome b_5, the kinetics of refolding and unfolding are more complex and exhibit very different transition states. The data support a model for unfolding in which heme−protein interactions give rise to two discernible rates of unfolding. From an analysis of the activation parameters associated with each process it is established that two structurally similar transition states differing by less than 5 kJ mol^{-1} exist in the unfolding reaction. Protein refolding exhibits monophasic kinetics but with distinct curvature apparent in plots of ln k_{obs} versus denaturant concentration. The data are interpreted in terms of alternative routes for protein folding in which a "fast track" leads to the rapid ordering of structure around Trp26 for refolding while a slower route requires additional reorganization around the hydrophobic core.

Proteins containing less than 100 amino acid residues frequently fold with rates ranging from 1 to 1000 s^{-1} in processes involving the translation of the primary sequence into an organized three-dimensional structure. Understanding the kinetic events associated with folding has represented a major experimental problem, although it has been shown, for example, that the small serine protease inhibitor CI2 denatures and refolds reversibly with kinetics and equilibria explained by a simple two-state model *(1, 2).* In other proteins such as barnase a more complex refolding pathway involving a transient intermediate, which is not sufficiently stable to be detected by equilibrium measurements, is formed as part of the overall process *(3).* Some proteins, such as staphylococcal nuclease or lysozyme, exhibit additional minor phases in refolding stopped-flow experiments, and this has led to the idea of conformational heterogeneity in unfolded states of the protein. This heterogeneity is attributed to the presence of cis and trans forms of prolyl peptide bonds and in staphylococcal nuclease the removal of the Pro residue by site directed mutagenesis resulted in simpler refolding kinetics *(4, 5).* Protein unfolding has been studied less often and for most small soluble domains the process exhibits monophasic kinetics *(6).* This is often explained is the transition-state model by an energy barrier that lies close to the folded or native conformation *(7).* However, some exceptions to the rule of single-exponential unfolding have been noted. Staphylococcal nuclease shows a biphasic profile upon denaturant induced unfolding *(8).* NMR[1] and kinetic studies indicate that a slow interconversion of native states that differ in their conformation about a single Pro peptidyl bond can account for these results *(9).* This observation is not restricted to staphylococcal nuclease and has been noted in calbindin D_{9k}, where NMR spectroscopy has identified major and minor conformers in solution *(10).*

Proteins containing a cofactor represent an interesting extension to the folding problem since complete folding requires the integration of the prosthetic group. In this context studies of the mechanism of unfolding and refolding in heme

[†] This work was supported by grants from the Wellcome Trust and BBSRC. The BBSRC is thanked for studentship support to both S.M. & G.M.

* Corresponding author: email D.Whitford@qmw.ac.uk; tel 44-171-9826349, fax 44-181-9830531.

[1] Abbreviations: GuHCl, guanidine hydrochloride; k_u/k_f, observed rate constant for protein unfolding/folding; k_{uw}/k_{fw}, first-order rate constant for protein unfolding or folding extrapolated to zero denaturant concentration; Ala1−Lys90 and Ala1−Ser104, soluble domain of cytochrome b_5 encompassing residues 1−90 or 1−104; NMR, nuclear magnetic resonance spectroscopy; m_{eq}, dependence of the free energy of unfolding on [GuHCl]; m_{ku}/m_{kf}, the dependence of the rate of protein folding/unfolding on [GuHCl]; ΔC_{pu} /ΔC_{pf} , heat capacity change associated with protein unfolding/folding.

10.1021/bi991413j CCC: $18.00
Published on Web 10/05/1999

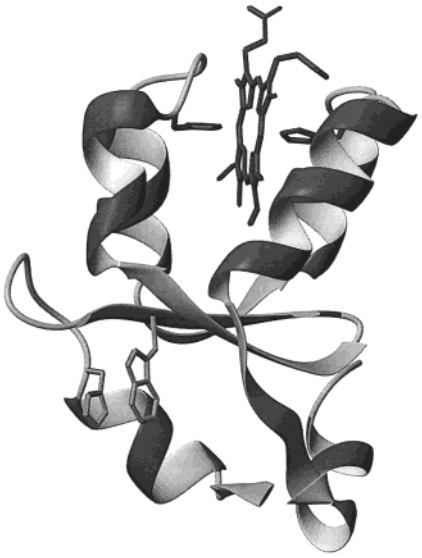

FIGURE 1: Ribbon diagram of the three-dimensional structure of the soluble heme binding fragment of cytochrome b_5. The diagram shows the single Trp residue at position 26 in the second hydrophobic core and its interaction with His19. The heme group ligated to the side chains of His 43 and 67 is also shown. The major elements of secondary structure are shown as helices and strands, and the diagram was prepared with the program Molmol *(65)*.

proteins have focused mainly on *c*-type cytochromes and particularly the homologous mitochondrial variants from yeast and horse as well as the structurally similar cytochrome c_2 from photosynthetic bacteria such as *Rhodobacter capsulatus (11)*. For horse heart cytochrome *c*, optical and NMR methods have established a complex folding pathway. The folding pathway contains several kinetic intermediates *(12)* with the rapid formation (<1 ms) of nativelike secondary structure detected by optical methods. In comparison studies of folding for *b*-type cytochromes have been limited and, in part, this is attributable to the ease with which the noncovalently bound heme group is lost to form the apoprotein. Unlike *c*-type cytochromes, where the cofactor is attached to the protein via covalent thioether bridges, all *b*-type cytochromes exhibit a slow loss of heme that can be measured in the reaction with apomyoglobin *(13)*.

One of the best-characterized *b*-type hemoproteins is microsomal cytochrome b_5, found in all eukaryotic cells *(14)*. In vivo, cytochrome b_5 is anchored to the endoplasmic reticulum membrane, although most studies have utilized fragments derived by limited proteolysis of the full-length protein *(15)* or via recombinant protein expression *(16−18)*. In general these fragments bind the heme within a soluble domain of 82−104 residues, with some recombinant forms of cytochrome b_5 retaining residues that are frequently lost from the amino terminus by proteolytic isolation methods. These residues can modulate the overall thermal stability of the protein in both the reduced and oxidized states *(18, 19)*.

Crystallography and NMR spectroscopy have provided data on the structure of the holo and apo forms of cytochrome b_5 *(20−24)*. In the holoprotein, both techniques point to similar tertiary structures with the heme group surrounded by four short helices (residues 38−43, 47−53, 58−65, and 70−75) and located on a platform formed by three well-defined β strands (residues 24−29, 32−37, and 56−58; Figure 1). It is held noncovalently via two imidazole side chains (residues 43 and 67), leading to a low-spin ferric center and a macrocycle that, in comparison with most *c*-type cytochromes, is relatively exposed to the solvent *(25)*. The heme macrocycle exists in two conformations that differ by rotation about the C5/C15 axis. In cytochrome b_5 the ratio of each isomer varies from species to species, ranging from approximately 25:1 in chicken to 9:1 in bovine and 1:1 in tobacco forms of the protein *(26−28)*. Spectroscopic studies of apocytochrome b_5 indicate a lower overall stability when compared with the holo form and a structure in which the four helices surrounding the heme are relatively disordered while the β strands appear to remain intact *(29, 23)*. More recently, kinetic studies of folding in apocytochrome b_5 have shown that the system exhibits kinetics that can be effectively modeled by the two-state approximation *(30)*. A pivotal reaction in the folding of apocytochrome b_5 was the formation of ordered structure around Trp26.

Currently it is unclear whether folding of holocytochrome b_5 proceeds via an apolike structure in which the Trp26 core is a transiently stable intermediate. There have been comparatively few mechanistic studies of folding/unfolding in holocytochrome b_5 although the globins have been the subject of many folding studies, especially in the apo state, as well as cytochrome b_{562} from *Escherichia coli (31−34)*. Unfolding in myoglobin has been shown to occur with multiphasic kinetics when initiated by rapidly lowering the pH, but it is also complicated by slow, irreversible heme aggregation *(32)*. The study of apoproteins does not allow the role of the heme group in modulating the stability of the protein and its rate of folding to be assessed. In this context optical studies of myoglobin unfolding in GuHCl for the cyanomet, deoxy, and met states have shown that heme coordination and oxidation states strongly influence the stability of the protein and the application of two state unfolding models *(35, 36)*. Alterations in the CD spectra of metmyoglobin upon GuHCl-induced denaturation indicates the presence of a stable intermediate and this has been equated to the molten globule state detected during acid induced unfolding of native myoglobin *(37)*. In cytochrome b_{562}, although the kinetics of folding/unfolding have not been analyzed extensively, it has been shown that the stability of apocytochrome b_{562} is substantially lower than the holoprotein when studied by differential scanning calorimetry, while NMR studies suggest the apo form retains a molten globule structure *(33, 38)*.

Unlike the globins and cytochrome b_{562}, the heme group in cytochrome b_5 has bis-histidine ligation, with the fifth and sixth positions occupied by two imidazole side chains and the native protein limited to low-spin d5/d6 states for the iron centers. The monomeric nature of the heme binding fragment of cytochrome b_5, its small size, and its relatively straightforward purification make this system a useful model for proteins whose correct assembly requires cofactor addition. Fortunately bovine cytochrome b_5 also lacks cysteine and methionine residues, and problems associated with disulfide bridge formation or side-chain oxidation can be discounted. This paper is part of an effort to define the conformational stability and folding/unfolding reactions of the holo form of cytochrome b_5. It focuses on examining the denaturation pathway of the best-characterized form of the protein; namely, the folded native state. To date holo forms of b hemoproteins have been poorly described in terms of both the kinetics and equilibria associated with denaturation. It is not clear if folding and unfolding proceed via

similar pathways, but with the recent characterization of the folding of apocytochrome b_5 the potentially more complex pathways associated with folding of the holoprotein can now be advanced *(30)*. In this study we show that although equilibrium studies suggest a two-state model for unfolding of holocytochrome b_5, kinetic studies reveal a more complex pattern of folding.

EXPERIMENTAL PROCEDURES

Construction of Protein Variants. The Ala1−Lys90 and Ala1−Ser104 variants of cytochrome b_5 containing the first 90 or 104 amino acid residues of bovine microsomal cytochrome b_5 were constructed by PCR methods from a template that represented a soluble fragment of cytochrome b_5 previously cloned and expressed in this laboratory *(18)*. The Ala1−Ser104 variant used in this study differed from that previously characterized by the introduction of a *Nco*I site around the start codon that facilitated subsequent cloning of the PCR product directly into pET21d. In all other respects this DNA sequence is identical to that described previously. The Ala1−Lys90 derivative was derived by PCR methods except that the following reverse primer (5′-G GTG AAG CTT ATT ATT CTG ATC TGT CAT CCG G-3′) containing a *Hind*III restriction site and two in-frame stop codons was used. This product, when inserted into pET21d, enabled the high-level expression of a soluble domain containing the first 90 residues. This was confirmed by DNA sequencing and SDS−PAGE/mass spectrometry of the purified product.

Protein Purification and Expression. The expression of cytochrome b_5 (Ala1−Ser104 and Ala1−Lys90) involved growing the cells aerobically at 37 °C in 500 mL of TYP medium (12 g/L tryptone, 24 g/L yeast extract, 2.3 g/L KH_2PO_4, and 12.5 g/L K_2HPO_4) with 100 μg/mL ampicillin. The cells were grown until the absorbance of the culture at 600 nm was 0.5, at which point IPTG was added to a final concentration of 0.5 mM. The cells were grown for a further 14 h and harvested by centrifugation at 5000*g* for 20 min. The cell pellets had a distinctive red coloration and were frozen at this stage at −20 °C after resuspension of the pellets in 50 mM Tris-HCl, pH 8.0, and 2 mM EDTA. Purification of cytochrome b_5 necessitated cell lysis and was performed as described previously *(18)*. The final fractions of cytochrome b_5 were a single homogeneous band when analyzed by SDS−PAGE and the molecular mass of each protein was determined by electrospray mass spectrometry to be within 20 amu of the expected value.

Equilibrium Unfolding Experiments. Solutions of GuHCl were made gravimetrically and further checked by refractive index measurements *(39)*. The protein concentration was determined in all experiments by the absorbance at 412.8 nm for the oxidized state of cytochrome b_5 and an extinction coefficient of 117 mM^{-1} cm^{-1}. Equilibrium absorbance measurements were performed on a Hewlett-Packard HP8452A photodiode array spectrophotometer equipped with a Peltier temperature controller. Cytochrome b_5 (1−3 μM) was incubated with 30 mM MOPS, pH 7.0, and concentrations of GuHCl between 0 and 7 M. The samples were allowed to equilibrate at 25 °C for 60 min prior to spectrophotometric measurements that involved recording the absorbance at 412 nm. Fluorescence measurements of protein denaturation were measured with a Perkin-Elmer LS-50 luminometer. All measurements were performed in a temperature controlled cuvette holder at 25 °C at a protein concentration of 3.0 μM in 30 mM MOPS, pH 7.0, and concentrations of denaturant between 0 and 7 M. For measurements of Trp fluorescence an excitation wavelength of 280 nm (slit width 5 nm) was used with the emission spectra recorded between 320 and 400 nm. The emission at 350 nm was plotted as a function of denaturant concentration to estimate the extent of protein unfolding. For both fluorescence and absorbance measurements, pre- and post-denaturation regions could be clearly identified and the equilibrium concentration of unfolded protein was determined by fitting the experimental data to

$$F = F_N - (F_N - F_U)\exp\{m_{eq}[\mathrm{GuHCl}] - \Delta G_{uw}/RT\}/\{1 + \exp\{m_{eq}[\mathrm{GuHCl}] - \Delta G_{uw}/RT\}\} \quad (1)$$

From this plot the parameters m_{eq} and ΔG_{uw} were estimated directly.

Kinetic Measurements of Protein Unfolding. All kinetic measurements of protein unfolding were performed on an Applied Photophysics stopped-flow SX18.MV system. A 150 W xenon arc lamp and a single monochromator (slit width corresponding to 4.65 nm) were used for both fluorescence and absorbance measurements. Changes in absorbance were measured at 412.8 nm with the 2 mm and 10 mm light paths. Fluorescence data sets were recorded with a 2 mm path length and with the intensity measured at 90° to the excitation wavelength (280 nm) after passing through a 320 nm cutoff filter. Data were collected over time intervals ranging from 50 ms to 1000 s with 1000−4000 data points. Each data point at a given denaturant concentration is the average of five successive traces. No additional noise filtering was applied to the data, and at 25 °C the dead time of the system by asymmetric mixing was determined to be ∼2.5 ms. All data were fitted with software supplied by Applied Photophysics Ltd.

Unfolding kinetics were measured at 25 °C and involved mixing 1 volume of native protein with 5−10 volumes of guanidine hydrochloride in 30 mM MOPS, pH 7.0. The denaturant concentration varied from 2.5 to 7 M. All unfolding and refolding reactions were independent of the final concentration of cytochrome b_5 (over a range from 0.2 to 5 μM) and were routinely performed at a protein concentration of 1 μM. Refolding kinetics were measured at 25 °C by mixing 1 volume of unfolded protein with 2−10 volumes of 30 mM MOPS, pH 7.0. The protein was initially unfolded by placing the sample in a high concentration of GuHCl (>3.5 M) for 1 h. The final denaturant concentration ranged from 0.27 to 2.8 M GuHCl. To assess whether the initial conditions influenced refolding rates and to overcome the limited number of mixing ratios available in stopped-flow experiments, an alternative folding procedure was used. Dilution into buffer containing low concentrations of GuHCl (<0.7 M) allowed the preservation of final folding conditions yet allowed the initial starting point to be varied between 4.5 and 7.0 M GuHCl. Results were obtained with the second procedure were identical to those obtained by the normal method of refolding. The rate of unfolding/refolding in the absence of denaturant was obtained by linear regression of semilogarithmic plots of equations of the type

$$\log k_u = \log k_{uw} + m_u[\text{GuHCl}] \quad (2)$$

where $m_{ku} = RTm_u$ and k_{uw} is the unfolding rate in water.

Determination of the Temperature Dependence of Protein Unfolding and Refolding. The temperature dependence of protein unfolding was studied over a range from 10 to 40 °C. The unfolding of cytochrome b_5 was determined at seven different denaturant concentrations between 3.6 and 5.8 M, with the change in fluorescence above 320 nm as a probe of protein unfolding. For each data set the rate of protein unfolding in the absence of denaturant (k_u) was determined by extrapolation of the data via semilogarithmic plots of k_{obs} versus denaturant concentration obtained at different temperatures. The values determined for k_{uw} were then used to calculate the activation parameters for protein unfolding via Eyring plots. For all data sets the temperature was controlled to within ±0.1 °C through the use of a Neslab RTE−111 thermocirculator. The temperature dependence of the rate of protein unfolding was fitted to eq 3, derived from transition-state theory *(40)*:

$$\ln (k_u/T) = \ln (k_b/h) + \Delta S_u^{\ddagger}/R - \Delta H_u^{\ddagger}/RT \quad (3)$$

Protein refolding was studied over a similar temperature range and the values of k_{fw} were plotted against $1/T$ in an Eyring-type analysis. For refolding eq 3 was modified to consider potential contributions of ΔC_p in the refolding reaction as seen for apocytochrome b_5 *(30)*:

$$\ln (k_f/T) = \ln (k_b/h) + \Delta S_f(T_0)/R - \Delta H_f(T_0)/RT - \Delta C_p (T - T_0)/RT + \Delta C_p/R \ln (T/T_0) \quad (4)$$

RESULTS

The unfolding of recombinant cytochrome b_5 exploits the fluorescence of the single Trp residue at position 26 as well as the absorbance attributable to correct ligation of the heme within the hydrophobic pocket. The relative positions of these groups within the soluble heme binding fragment are shown in Figure 1, with the heme and Trp residue separated by a distance of ∼12 Å. In the folded state both apo and holo forms show a low level of Trp fluorescence resulting from quenching by His19 *(20, 41)*.

Equilibrium Denaturation of Cytochrome b_5. The unfolding transition is followed by either absorbance or fluorescence measurements. In the soluble domain of cytochrome b_5, Trp26 acts as a convenient and sensitive reporter of the folded state with changes in the fluorescence intensity occurring in the presence of denaturants. In the native protein the fluorescence at 350 nm associated with the Trp residue is relatively low and a maximum around 330 nm is apparent as observed in studies of apocytochrome b_5 *(30)*. However, the addition of elevated concentrations of GuHCl to Ala1−Ser104 cytochrome b_5 leads to an increase in fluorescence intensity at 350 nm, as shown in Figure 2. At concentrations of denaturant below 2.0 M the fluorescence emission at 350 nm remains low but increases progressively, reaching a maximum at approximately 4.5 M GuHCl. Above this concentration no further changes in fluorescence are detected. The reversibility of this change was ascertained by performing the titrations in both folding and unfolding directions, which yielded identical denaturation curves. In comparison

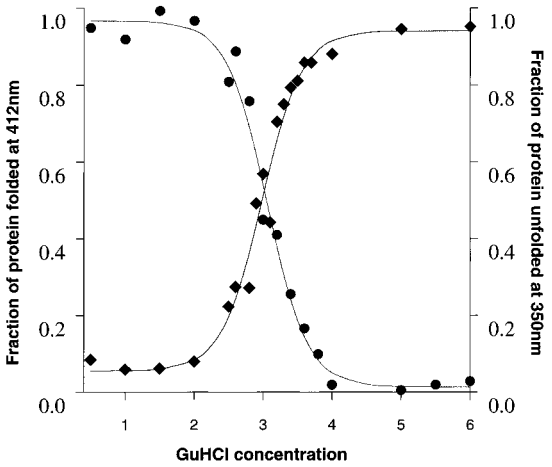

FIGURE 2: Equilibrium-based measurements of GuHCl-induced unfolding of Ala1−Ser104 cytochrome b_5. (◆) Fluorescence data; (●) absorbance data. All measurements were performed at a protein concentration of 3 μM, in 30 mM MOPS, pH 7.0, and at 25 °C. The data were fitted to the lines shown by use of eq 1.

with the fluorescence data, the absorbance at 412.8 nm decreases with elevated denaturant concentrations and progressively shifts to yield a maximum at 395 nm at high concentrations of denaturant. The absorbance maximum in this region is similar to that exhibited by free heme in 6 M GuHCl and may reflect the loss of bis-histidine ligation within the heme binding pocket of cytochrome b_5. From absorbance spectra a denaturation curve can be defined with the profile remaining at a maximal value up to ∼2 M GuHCl and then declining sharply before reaching a minimum around 4.5 M GuHCl. It is clear that the transition midpoint for both the absorbance and fluorescence data sets are coincident and that both reporter groups delineate a single transition in which intermediates are not detected. For each curve pre- and posttransitional regions can be identified, and values of m_{eq} and ΔG_{uw} of ∼8800 J mol^{-1} M^{-1} and 26.5 kJ mol^{-1} are estimated via eq 1.

Kinetic Measurements of Protein Unfolding. The fluorescence intensity of Trp26 changes upon mixing cytochrome b_5 with denaturing concentrations of GuHCl. The time-dependent changes in fluorescence (λ > 320 nm) show an increase as the protein unfolds and are complete within ∼500 ms at a denaturant concentration of 5 M GuHCl. The change is best described as the sum of two exponential processes. This is emphasized in the residual plots for both mono- and biexponential processes where the error, especially during the first 100 ms, is more pronounced in the monoexponential fit (Figure 3A). The ligation of the heme by two imidazole side chains in ferricytochrome b_5 yields an intense absorbance band at 412.8 nm that is a useful monitor for the integrity of the heme pocket. It is observed that under denaturing conditions ([GuHCl] > 3 M) the absorbance at 412.8 nm decreases with time. This profile is again best fitted as the sum of two exponential rates, and at all denaturant concentrations the observed rates are identical to those seen with fluorescence (Figure 3B). The amplitudes associated with the two kinetic phases represent 30% (A_1) and 70% (A_2) of the total fluorescence (or absorbance) change, and in view of the proportion of the fast phase it is clear that this represents a kinetically significant reaction. The amplitudes associated with these two processes do not vary at denaturant

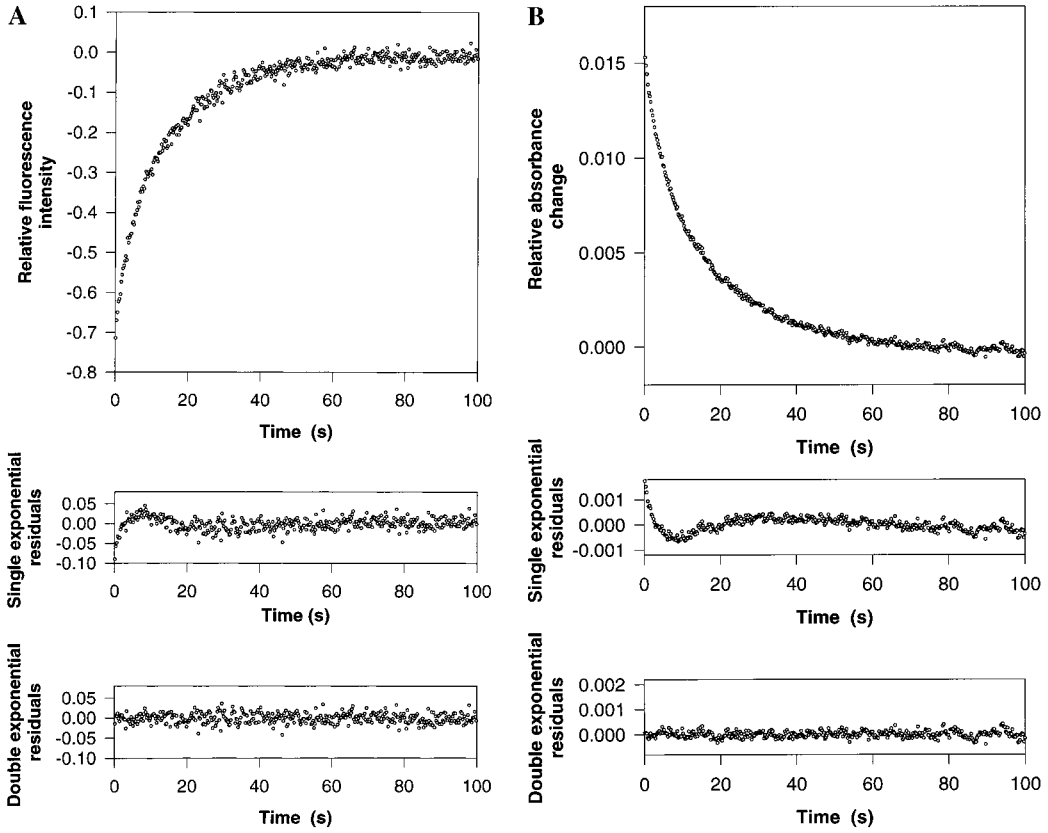

FIGURE 3: Transient changes in (A) fluorescence and (B) absorbance for the unfolding of Ala1−Ser104 cytochrome b_5. The data were recorded by following the change in fluorescence at wavelengths greater than 320 nm as a result of mixing the folded protein with 10 volumes of GuHCl (final concentration 4.8 M) in 30 mM MOPS, pH 7.0. The final protein concentration was 1 μM. Further changes in fluorescence were not detected at longer time intervals. The data shown are fitted to the sum of two exponential processes with amplitudes for the fast and slow phase representing ~30% and ~70% of the total change. The residuals plots for mono- and biexponential processes are shown below the kinetics trace and emphasize the superior fit to a biexponential process. The absorbance data were recorded under similar conditions to those described for the fluorescence changes. Quantitatively identical results were obtained with this probe for protein unfolding.

concentrations above 4 M GuHCl, as shown in Figure 4, with the variation of each phase remaining constant to within approximately ±5%. However, below 4 M GuHCl, in a region corresponding to the transition zone of Figure 2 it is observed that the fast and slow phases alter dramatically in their relative proportions. The faster phase becomes the dominant process while the slow phase declines from a maximum of 70% of the total amplitude to less than 30% of the total change. More importantly the sum of the amplitudes of the two phases observed from the absorbance at 412 nm ($A_1 + A_2$) corresponded to the total change observed in equilibrium studies and accounts for all of the protein on the basis of the known extinction coefficient of cytochrome b_5. This result suggests that transient absorbance changes within the dead time of the instrument (under these conditions ~2 ms) do not occur. The folding kinetics in the transition region are complex and were not characterized in further detail in this study.

Alongside the variation in the amplitudes associated with each unfolding process, the change in their respective rates as a function of denaturant concentration were also determined. From the data of Figure 4 the fast and slow kinetic phases exhibit a linear dependency on denaturant concentration, and by extrapolating the data to zero denaturant the intrinsic unfolding rate constants (k_{uw}) were estimated. For the fast and slow phases, unfolding rates (k_{uw}) of $(4.5 \pm 0.6) \times 10^{-5}$ s^{-1} and $(5.2 \pm 0.6) \times 10^{-6}$ s^{-1} are estimated at 25 °C. Identical values are calculated from either absorbance or fluorescence data sets, and both processes exhibit a similar dependence on GuHCl concentration with values of $m_{\ddagger-F}$ of 5300 and 5400 J mol^{-1} M^{-1}. At the highest concentrations of GuHCl each plot exhibits a very slight curvature. The $m_{\ddagger-F}$ value represents the dependence of $\Delta G_{\ddagger-F}$ on denaturant concentration and is proportional to the change in solvent exposure of the protein as the structure shifts from the native to transition states *(3, 42)*. The calculated values of m_{ku} and m_{eq} are shown in Table 1 and indicate the position of the transition state on the reaction coordinate between the folded and unfolded states through an estimation of the ratio $m_{\ddagger-F}/m_{U-F}$. In this study the ratio ranges from 0.6 to 0.62 over a theoretical range of 0−1, where 0 indicates a structure close to the folded form of the protein and the preservation of noncovalent interactions, while 1 indicates a transition state resembling that of the unfolded or disordered state. The similar values obtained by fluorescence and absorbance suggest that these probes are monitoring the same global unfolding process.

Analysis of Kinetic Heterogeneity by Use of Different Variants of the Soluble Heme Binding Domain. In view of the known sensitivity of cytochrome b_5 to proteolysis during isolation, it remains important to ascertain that the kinetic heterogeneity observed during unfolding was not attributable to forms of cytochrome b_5 truncated at the N and C termini and therefore differing in their sensitivity to GuHCl. To gain

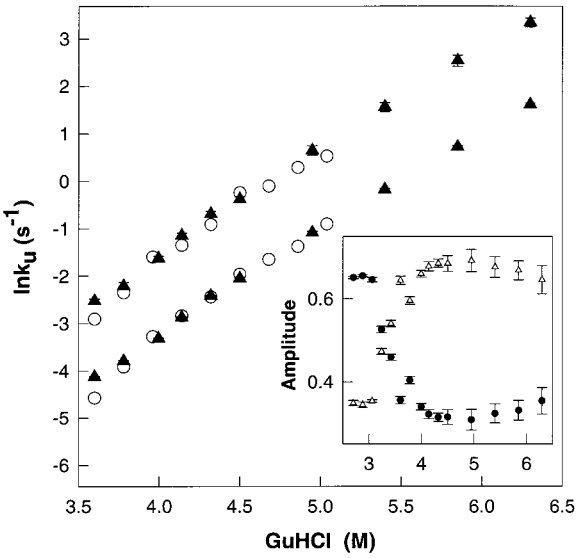

FIGURE 4: Semilogarithmic plot of the dependency of unfolding rates on denaturant concentration for Ala1−Ser104 cytochrome b_5 along with the variation of the amplitude of the fast and slow phases. At zero denaturant concentration the rates of unfolding for each process are $(4.5 \pm 0.6) \times 10^{-5}$ s^{-1} and $(5.2 \pm 0.6) \times 10^{-6}$ s^{-1}. The open symbols denote the rates measured from changes in the absorbance at 412.8 nm, while the solid symbols are the rates obtained from fluorescence measurements for the two-exponential processes. The inset shows the amplitudes associated with each phase. The amplitudes of the fast (●) and slow phase (△) change significantly within the transition zone but are constant (±5%) above 4.0 M. At high denaturant concentrations (>5.5 M) the rapid changes in fluorescence make accurate digitization of the data difficult and lead to proportionally larger errors.

Table 1: The Free Energy Changes Associated with Unfolding of Ala1−Ser104 Cytochrome b_5[a]

	ΔG_{uw} (kJ mol^{-1})	m_{eq} or m_{ku} (J mol^{-1} M^{-1})	[GuHCl]$_{0.5}$ (M)
Equilibrium			
absorbance	27.5 ± 3.3	8950 ± 1100	3.05 ± 0.1
fluorescence	25.5 ± 3.5	8560 ± 1200	2.99 ± 0.1
Stopped Flow			
absorbance fast	25.9 ± 2.1	5379 ± 570	
absorbance slow	31.5 ± 1.0	5404 ± 570	
fluorescence fast	24.0 ± 0.8	5156 ± 124	2.9 ± 0.1
fluorescence slow	29.3 ± 1.4	5404 ± 224	3.2−3.5

[a] All data were obtained at 25 °C in 30 mM MOPS, pH 7.0. Similar values for the fast and slow components may be determined from either fluorescence or absorbance measurements. The average values of ΔG_{uw} are 25.0 ± 1.5 and 30.4 ± 1.2 kJ mol^{-1}, while the respective m_{ku} values are 5268 ± 347 and 5404 ± 397 J mol^{-1} M^{-1}. These values may be compared with the average values of 26.5 ± 3.4 kJ mol^{-1} and 8755 ± 1150 J mol^{-1} M^{-1} for the conformational stability and dependence of ΔG_{uw} on denaturant concentration obtained from equilibrium measurements.

further insight into the mechanism of protein unfolding we have examined the rate of GuHCl-induced unfolding in a second variant of cytochrome b_5 containing the first 90 residues. This variant, designated Ala1−Lys90 cytochrome b_5, exhibits identical kinetic behavior to the longer Ala1−Ser104 variant with fast and slow rates of similar magnitude and amplitude (see Supporting Information). Further studies have involved the use of a deletion variant lacking five residues at the N terminus, as well as a mutant in which Pro44 was replaced by alanine. Both proteins exhibited biphasic profiles during kinetic unfolding experiments (Manyusa and Whitford, 1998, unpublished results). The similar rates and amplitudes associated with protein unfolding, coupled with their similar denaturant dependency, points to an origin for the observed kinetic heterogeneity that lies within the heme binding domain, i.e., residues 7−90, of cytochrome b_5 and does not involve the N- and C-terminal regions.

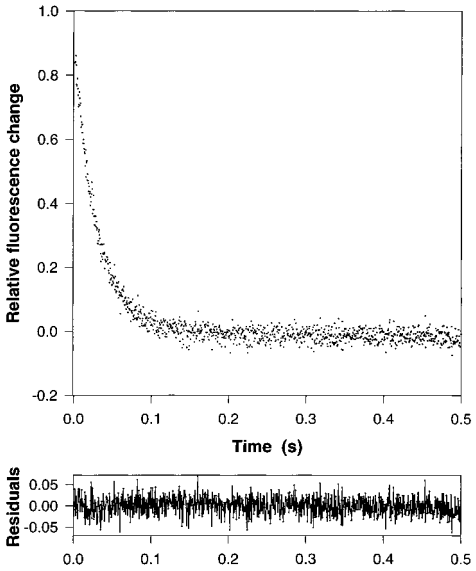

FIGURE 5: Kinetics of Trp fluorescence quenching during refolding of holocytochrome b_5. The fluorescence (λ > 320 nm) was recorded over a time period of 500 ms by mixing 1 volume of denatured protein, prepared as described in the Experimental Procedures section, with 10 volumes of 30 mM MOPS, pH 7.0. The data are shown fitted to a monoexponential process.

Kinetics of Refolding of Cytochrome b_5 Followed by Trp Fluorescence. The denaturation of holocytochrome b_5 at high concentrations of GuHCl leads to a form of the protein in which the solitary tryptophan residue is exposed to the solvent and exhibits maximal fluorescence at wavelengths around 350 nm. Protein refolding is initiated by rapidly mixing the protein under solution conditions favoring formation of the native state (GuHCl < 2.5 M). Refolding is observed by a rapid decrease in the fluorescence emission above 320 nm with time (Figure 5). The decrease in fluorescence is a single-exponential process, as emphasized by the residuals plot, and there is no evidence for a second process, in contrast to that observed during the unfolding of cytochrome b_5. The observed rates do not depend on the initial unfolding conditions over the range 4.0−7.0 M GuHCl, with identical rates observed at the same final denaturant concentration. These data can be extended to measure the variation in the rate of refolding at different final denaturant concentrations. These data, when combined with the denaturant dependence of the unfolding rate, lead to a characteristic "chevron plot", in which unfolding and folding regions are clearly delineated. From Figure 6 the transition region is centered at 2.9 M GuHCl, in close agreement with that detected from equilibrium studies.

The transition region is most clearly defined by the faster of the two unfolding phases, where the unfolding and refolding rates become very similar at denaturant concentrations of ~3.0 M. The slower unfolding phase appears to intersect with the refolding limb at approximately 3.2−3.5 M and the relevance of this concentration to the current

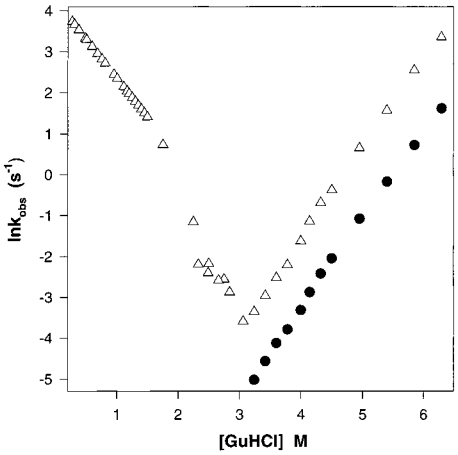

FIGURE 6: Chevron plot showing the dependence of refolding and unfolding rates on denaturant concentration. The data defining the fast (●) and slow phase (△) of unfolding are shown together with data on the refolding reaction. Two refolding regions are clearly distinguished in the current plot between 0 and 1.4 M and between 1.4 and 2.8 M GuHCl. The two regions can be seen in more detail in the Supporting Information. The extrapolated rate constants and *m* values associated with each reaction are described in Table 2.

Table 2: Thermodynamic and Kinetic Data for the Folding and Unfolding Reactions of Ala1−Ser104 Cytochrome b_5[a]

folding transition	m_k or m_{eq} (J mol^{-1} M^{-1})	ΔG_{uw} or ΔG_{fw} (kJ mol^{-1})
unfolding fast	5156 ± 124	24.0 ± 0.8
unfolding slow	5404 ± 224	29.3 ± 1.4
refolding 1	8517 ± 518	−17.6 ± 0.6
refolding 2	3978 ± 329	−10.1 ± 0.2
equilibrium	8560 ± 1200	25.5 ± 3.5

[a] All of the kinetic data were obtained from measurements of the fluorescence changes above 320 nm as described in the Experimental Procedures section. The individual values for the two refolding regions were obtained from linear regression of the data in two separate regions (0−1.4 M and 1.5−2.8 M).

profile and that observed at equilibrium remains unclear. By measuring refolding over much longer time intervals (100 s) it was possible to rule out additional slow phases attributable to rate-limiting proline isomerization since no further fluorescence changes occurred within this time scale. The folding limb shows evidence of two distinct processes. The faster process is observed above 1.4 M, and by extrapolating the data to zero denaturant concentration a maximal rate of ∼1200 s^{-1} is estimated for this process. In contrast, the reaction occurring below 1.4 M GuHCl has a slower rate in the absence of denaturant of ∼60 s^{-1}. The dependence of the refolding rate on denaturant concentration (m_{kf}) for each process differs significantly, and by fitting the data obtained between 0 and 1.4 M GuHCl and between 1.5 and 3.0 M GuHCl, values for m_{kf} of ∼4000 J mol^{-1} M^{-1} and 8500 J mol^{-1} M^{-1} are estimated (Table 2). The second of these values is somewhat surprising since its magnitude is comparable to the equilibrium value obtained for unfolding (8800 J mol^{-1} M^{-1}) and the sum of the kinetic *m* values should clearly equal that for the complete unfolding reaction in a two-state process.

Temperature Dependence of Protein Folding and Unfolding Reactions. By measuring changes in the rate of protein unfolding with temperature, the activation parameters were defined via an Eyring-type analysis. The rates of unfolding (k_{obs}) at seven different GuHCl concentrations were measured at temperatures between 11 and 40 °C, and two rates were observed throughout this range. The rate of unfolding at zero denaturant concentration was calculated at each temperature and used in eq 3 to estimate values of $\Delta S_u^{\ddagger}$, the activation entropy associated with protein unfolding, and $\Delta H_u^{\ddagger}$, the activation enthalpy of protein unfolding. Over a temperature range of 29 K such plots were linear, and this generally indicates that the change in heat capacity (ΔC_{pu}) between the native and transition state for protein unfolding is small (Figure 7A). The values derived from Figure 7A for the activation enthalpy ($\Delta H^{\ddagger}$) and entropy ($\Delta S^{\ddagger}$) are similar for each phase. For the fast phase values of 165 ± 9 kJ mol^{-1} and 227 ± 31 J mol^{-1} K^{-1} are calculated, while for the slower phase the corresponding values are 167 ± 5 kJ mol^{-1} and 219 ± 17 J mol^{-1} K^{-1}. In view of the linearity of this plot it can be assumed that $\Delta H^{\ddagger}$ and $\Delta S^{\ddagger}$ are independent of temperature in this range, and this leads to an activation free energy of 97 and 101 kJ mol^{-1} at 25 °C for the fast and slow phases, respectively.

The temperature dependence of protein refolding is calculated for the slower reaction seen in the chevron plot of Figure 6 via an Eyring-type plot (Figure 7B). The data show that significant curvature is apparent in these plots, in contrast to that seen for protein unfolding. The curve was modeled with eq 4 and leads to values for the activation enthalpy of 43 kJ mol^{-1}, while a value for the entropy change upon refolding of −66 J mol^{-1} K^{-1} is estimated. The curvature apparent in the Eyring plot suggests that the heat capacity change ($\Delta C_{pu-\ddagger}$) between the unfolded and transition states is significant with a value of 4.5 J mol^{-1} K^{-1} estimated from fitting eq 4 to the data shown in Figure 7. This value is comparable to that estimated in the refolding reaction of apocytochrome b_5, and the activation parameters for unfolding and refolding are summarized in Table 3.

DISCUSSION

Equilibrium Unfolding Studies. Detailed equilibrium and kinetic studies of protein unfolding of holocytochrome b_5 have not been extensively described although Tajima et al. *(43)* reported a midpoint for denaturation of 2.9 M GuHCl for the tryptic fragment of rabbit cytochrome b_5 by using changes in CD and absorbance spectra. These data agree closely with those obtained here for longer fragments of the soluble domain of cytochrome b_5 by changes in Trp 26 fluorescence. In holocytochrome b_5 the fluorescence of Trp26 remains low, and structural studies indicate that most of the indole side chain is buried away from solvent and in close proximity to His19 *(20, 41)*. In equilibrium unfolding studies, disruption of the hydrophobic core around Trp26 is part of the same cooperative transition observed at the heme center. The conformational stability in the absence of denaturant (ΔG_{uw}) is 26.5 kJ mol^{-1}. This value agrees with that seen in other studies including thermal denaturation of the tryptic fragment of rabbit cytochrome b_5 *(44)*. Similar values were also derived for bovine cytochrome b_5 in thermal denaturation studies *(19)*, and this has been further verified by studies of recombinant forms of the rat and bovine proteins *(45, 46)*.

The dependency of ΔG on GuHCl concentration has not been widely reported for the soluble domain of cytochrome b_5, but here a value of 8800 J mol^{-1} M^{-1} has been derived

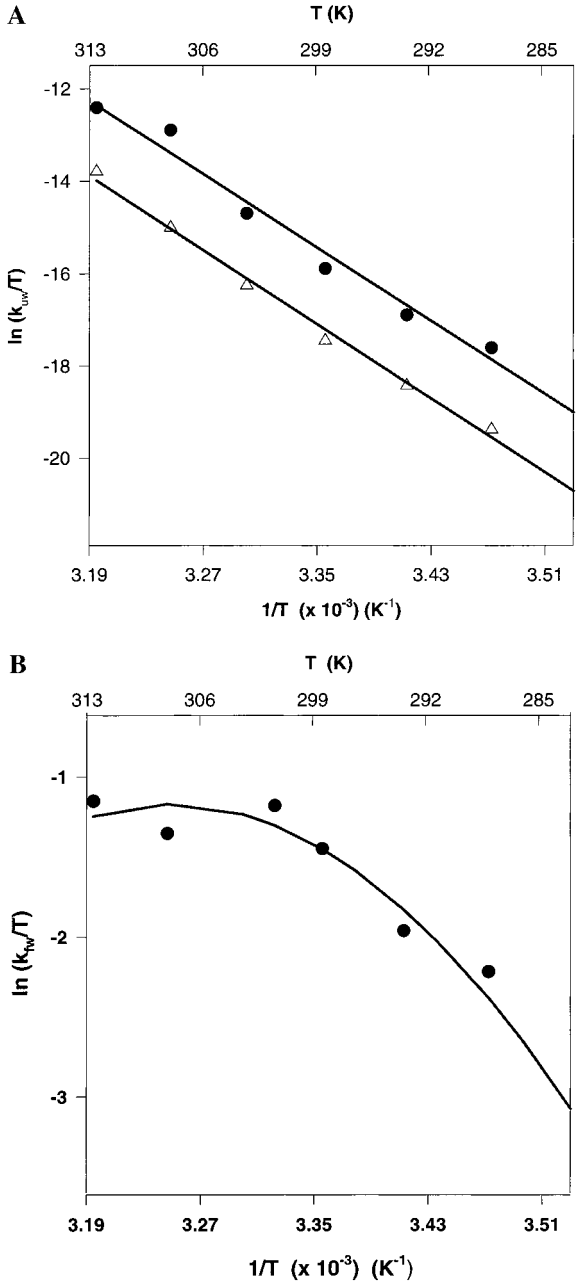

FIGURE 7: Eyring plots showing the temperature dependence of the (A) unfolding and (B) refolding rates (k_{uw}/k_{fw}) for Ala1−Ser104 cytochrome b_5. (A) The individual points were calculated by extrapolation of the linear plots of ln k_{uw} versus GuHCl concentration. The dependency of the unfolding rate on denaturant concentrations between 3.5 and 6.5 M was determined at six temperatures between 10 and 40 °C for the fast (●) and slow (△) unfolding processes. (B) The individual points were calculated by extrapolation of the linear plots of ln k_{fw} versus GuHCl concentration. The dependency of the refolding rate on denaturant concentrations between 0 and 1.5 M was determined at six temperatures between 10 and 40 °C.

from equilibrium unfolding data. A value of 3700 J $mol^{-1}M^{-1}$ was obtained for denaturation of a soluble domain of bovine cytochrome b_5 containing 82 residues with urea *(45)*, while denaturation of *full-length* rat cytochrome b_5 in the presence of urea gave a value of 0.67 kcal mol^{-1} M^{-1} (∼2800 J mol^{-1} M^{-1}) *(46)*. The *m* values obtained from denaturation with urea are often lower than those obtained with GuHCl and the observed differences (∼8800 vs 2800−3700 J mol^{-1} M^{-1}) are within the range reported for other systems *(47)*.

Table 3: Activation Parameters for the Unfolding and Refolding Reactions of Ala1−Ser104 Cytochrome b_5[a]

	$\Delta H^{\ddagger}$ (kJ mol^{-1})	$\Delta S^{\ddagger}$ (J mol^{-1} K^{-1})	$\Delta G^{\ddagger}$ (kJ mol^{-1})	$\Delta C_p^{\ddagger}$ (kJ mol^{-1} K^{-1})
unfolding fast	165 ± 9	227 ± 31	97.3	1.5[b]
unfolding (slow)	167 ± 5	219 ± 17	101.7	1.5[b]
refolding	43 ± 5	−65 ± 15	62.6	−4.5 ± 1.0

[a] The data shown above were calculated from the Eyring plots for the temperature dependence of the unfolding and refolding of Ala1−Ser104 cytochrome b_5. The activation parameters are those obtained at zero denaturant concentration in 30 mM MOPS, pH 7.0, and at 25 °C. The unfolding reaction shows the values of the activation parameters calculated for both processes. In view of the detectable curvature in the refolding curve the data were fitted to eq 4 to yield estimates of $\Delta H^{\ddagger}$ and $\Delta S^{\ddagger}$. [b] The value for $\Delta C_p^{\ddagger}$ was calculated with the value for ΔC_p of 6.0 kJ mol^{-1} K^{-1} estimated by differential scanning calorimetry *(29)* and the relationship $\Delta C_p = \Delta C_{pu} - \Delta C_{pf}$.

In the absence of other experimental values of m_{eq} for holocytochrome b_5, the data obtained for various metmyoglobins (10−15.5 kJ mol^{-1} M^{-1}) provide another comparison *(48)*. The lower value of m_{eq} is not surprising since the recombinant domains of cytochrome b_5 (90−104 residues) are smaller than myoglobin (153 residues), while ANS binding experiments suggest that the heme binding pocket of globins is substantially more hydrophobic than the comparable regions in cytochrome b_5 *(49)*.

Origin of the Kinetic Patterns of Protein Unfolding. All variants of the soluble domain of cytochrome b_5 used in this study unfold in the presence of GuHCl in a process that involves at least two exponential processes. The kinetic heterogeneity of cytochrome b_5 denaturation is unusual and departs from the monophasic unfolding patterns seen for single domains. Heterogeneity in unfolding has been observed in staphylococcal nuclease and calbindin D_{9k}, where cis−trans proline isomerization in the folded state have been shown to be the origin of biphasicity *(4, 10)*. However, in the unfolding of cytochrome b_5 it is unlikely that cis−trans isomerization is the origin of heterogeneous unfolding rates for a number of reasons. Ala1−Ser104 cytochrome b_5 contains three proline residues at positions 44, 85, and 96. Pro96 and 44 can be discounted since these residues have been eliminated by the use of shorter variants or mutants, and Pro85 remains the only candidate. In calbindin D_{9k} the interconversion between native states yields a fingerprint (NH/Hα) region in NMR spectra that contains cross-peaks representing major and minor conformers, and from exchange measurements the rate of interconversion has been estimated to be 0.1−0.01 s^{-1} *(10)*. This rate is comparable to that observed in model pentapeptides containing Pro residues and to that seen in protein systems known to exhibit a slow conversion between cis and trans conformations but remains very different from those observed in this study *(50, 51)*. Additionally, both the fast and slow rates show a linear dependency on the denaturant concentration in semilogarithmic plots at pH 7.0, whereas in other systems the slow phases frequently attributed to cis−trans Pro isomerization exhibit little or no dependence on denaturant concentration *(52)*.

Cytochrome b_5 has been studied extensively by homo- and heteronuclear NMR methods, and although heterogeneity has been detected for the heme environment, this does not extend to the protein domain *(53)*. Heteronuclear single quantum

coherence (HSQC) spectra do not indicate multiple conformations attributable to multiple conformations, nor does the crystallographic structure of the bovine fragment indicate cis peptide bonds preceding Pro44 and Pro85 *(21, 22)*. More significantly, apocytochrome b_5 does not exhibit biphasic unfolding despite an identical protein sequence, and this suggests that the heme and/or its interaction with the protein is the origin of the two kinetic phases seen in this study *(30)*. At equilibrium the ratio of major to minor heme isomers in recombinant bovine cytochrome b_5 is 9:1, in agreement with that first observed for the tryptic fragment of this protein *(18, 53)*. Further support for the origin of biphasic unfolding residing in the nature of the heme−protein interaction is seen from a comparison of the unfolding rate in the absence of denaturant with that measured for both heme transfer and heme reorientation. In ferricytochrome b_5 the two orientations for the heme in the hydrophobic pocket can be distinguished by ^{1}H NMR spectroscopy, with the rate of interconversion [$(1.6-3.0) \times 10^{-5}$ s^{-1}] strongly dependent on temperature and solution pH (*54*, *55*). Heme reorientation is assumed to proceed via at least partial unfolding to allow the rupture of both bonds between the Fe and imidazole ligands. The maximal rate of heme reorientation must therefore be slower than the intrinsic unfolding rate of cytochrome b_5 estimated in this study (4.5×10^{-5} s^{-1}). The rate observed for the fastest phase of unfolding is clearly commensurate with this reorientation rate although the slower, dominant phase is approximately an order of magnitude less. By a similar argument, the rate of heme dissociation must depend on initial unfolding events. Heme dissociation from proteins has been measured in biomolecular exchange reactions with apomyoglobin (*56*). For cytochrome b_5 this rate ranges from 8.3×10^{-5} s^{-1} to 1.7×10^{-5} s^{-1} in different recombinant fragments of the rat protein *(46, 56)*. The measured rate of heme transfer to apomyoglobin is again comparable to the fastest rate of protein unfolding obtained in the absence of denaturant and at lower temperatures (25 versus 37 °C). This suggests that the unfolding process is inextricably linked to the loss of heme and may represent the rate-limiting step in both heme reorientation and transfer. As expected in view of the stabilization of the protein by heme binding, the intrinsic unfolding rate for holocytochrome b_5 ($k_{uw} \sim 4.5 \times 10^{-6}$ s^{-1}) is much less than for the apo form of the protein ($k_{uw} \sim 0.2$ s^{-1}).

Although the molecular basis for biphasic unfolding remains to be elucidated, it has been clearly identified to the heme group and its interaction with the polypeptide. An insight into possible mechanisms of biphasic unfolding in cytochrome b_5 is suggested from studies of the denaturation of the rat soluble domain by one- and two-dimensional NMR studies *(57)*. Unfolding involves the breakage of many hydrogen bonds, and the bond between Ser68 NH and the heme C17 propionate is thought to be important. The patterns of protein unfolding described here are further enhanced by detailed structural studies of the two orientations of the heme in rat cytochrome b_5. In the rat protein orientation A is defined by the presence of a hydrogen bond between Ser68 and the heme C17 propionate, while orientation B lacks this bond and appears to be displaced 0.9 Å out of the heme pocket *(58)*. If we can extend these results to the major and minor orientations of bovine cytochrome b_5, then the fast unfolding phase could be equated to a conformation lacking hydrogen bonds, including the critical hydrogen bond between the Ser68 NH and the buried propionate group. Since the two conformers are known to have similar overall tertiary structures, it is significant that the activation parameters estimated for protein unfolding suggest two structurally similar and related transition states differing by less than 10 kJ mol^{-1}. However, as a caveat, it is also clear that the equilibrium ratio of heme conformers is not reflected in the amplitudes of the fast and slow unfolding phases, suggesting that separate unfolding pathways for each form of the protein are not the direct origin of biphasicity.

Energetics of Protein Unfolding. The activation energies ($\Delta G^{\ddagger}$) of ∼100 kJ mol^{-1} seen for each unfolding phase emphasize the small differences between the fast and slow phases (4.4 kJ mol^{-1}). This comparatively small energy difference suggests two transition states for each unfolding process that are very similar in their noncovalent interactions and solvent accessibility. The values of $m_{\ddagger-N}$ for the fast and slow phases are 5400 and 5300 J mol^{-1} M^{-1} and point to a ratio $m_{\ddagger-N}/m_{U-N}$ of approximately 0.60−0.62. The transition state for protein unfolding in this instance does not lie close to the native state and is approximately midway between the folded and denatured states. It is also significantly different from that seen in the unfolding of apocytochrome b_5 *(30)*. The slightly higher value of $m_{\ddagger-N}$ shown by the fast phase may reflect greater solvent accessibility in this protein conformer via the displacement of the heme out of the pocket as seen for the rat protein *(58)*. However, it should be noted that the two values are within experimental error of each other and the precise mechanism of biphasic unfolding remains to be elucidated. In addition the $\Delta(\Delta G)$ between the two processes is commensurate with that expected for two states differing by a small number of weak interactions and could represent the difference between the gain or loss of a single hydrogen bond. Similar differences in conformational stability (∼5 kJ mol^{-1}) have been noted between the major and minor isomers in both erythrocyte cytochrome b_5 and the trypsin-solubilized fragment of bovine cytochrome b_5 *(59)*. Thus in addition to conferring slightly different reduction potentials *(60)* the two orientations may also modulate the stability and unfolding of cytochrome b_5.

Refolding Monitored by Changes in Trp Fluorescence. It is clear that the overall refolding process exhibits a nonlinear dependence on GuHCl concentration. Refolding in holocytochrome b_5 exists as two clearly defined processes with rates that differ significantly when extrapolated to zero denaturant concentration (1200 s^{-1} and 60 s^{-1}). The dependence of each process on denaturant concentration also differs, with values of 8500 and 4000 J mol^{-1} M^{-1}. As noted earlier, the kinetic *m* value associated with the faster refolding process remains at odds with a simple two-state mechanism and is more representative of the complete folding reaction from unfolded to native states. In view of its magnitude it is possible that a rapid condensation of ordered structure forms around Trp26 in a proportion of the protein. This process is not observed during refolding of the apoprotein and clearly centers around the presence of the heme *(30)*. In contrast, the slower refolding rate is comparable to that seen in the apoprotein, suggesting they could represent similar reactions. The second process with a kinetic *m* value of ∼4000 J mol^{-1} M^{-1}, when combined with the *m* value calculated for the unfolding reaction (5200 J mol^{-1} M^{-1}), yields a value ($m_{ku} + m_{kf}$) of

9200 J mol^{-1} M^{-1}. This is similar within experimental error to the equilibrium *m* value determined previously (8800 J mol^{-1} M^{-1}). Further evidence for the potential similarity of the folding reactions are the comparable values of ΔC_p observed during refolding of the holo- and apoproteins as well as similar activation energies (Table 3; *30*).

It has become clear with recent refolding studies that aggregation can contribute to anomalous kinetic behavior *(61)*. This is unlikely in the present study since this effect was not observed during the refolding of apoprotein performed with very similar protein concentrations *(30)*. In addition, the refolding reactions of Figure 6 have been carried out at protein concentrations ranging from 0.2 to 5 μM and identical results have been obtained. This implies that protein aggregation is not a significant process under the present conditions. In this study the "anomalous" process appears to be a very rapid refolding event ($k_{uw} \sim 1200$ s^{-1}) that does not show a protein concentration dependence. A further test of aggregation is to plot the amplitudes as a function of concentration for the refolding process and again this remained linear under all conditions. Consequently we believe that the present refolding profiles reflect fast and slow formation of ordered structure around Trp26. The faster process involves the heme group and in many ways this behavior is similar to the fast and slow tracks of protein folding noted in other systems *(62)*. In studies of apocytochrome b_{562} it was found by use of isothermal titration calorimetry that the denatured protein could surprisingly bind the heme with a dissociation constant of approximately 3 μM, although this was much weaker than the corresponding value observed for the holoprotein (9 nM) *(63)*. This offered an alternative path for refolding of denatured apocytochrome b_{562}, where heme binding formed denatured holoprotein prior to formation of the native protein. These experiments were performed on thermally denatured apoprotein, and data on GuHCl denatured proteins remain to be obtained. Similarly, the binding of free heme to unfolded cytochrome b_5 remains to be measured. The changes in absorbance spectra at high denaturant concentrations suggest the disruption of bis-histidine ligation, although it remains possible that the heme is linked to the polypeptide via a single histidine residue or attached by other hydrophobic interactions. This is supported by the lack of dependence of refolding rates on protein concentration as well as their independence of initial GuHCl concentration.

For cytochrome b_5 the presence of a single Trp residue facilitates the interpretation of folding kinetics, and from the observed emission maxima at 330 and 349 nm it is clear that this residue is monitoring formation of the folded and unfolded states. Trp26 is buried in a solvent-inaccessible core in a coplanar orientation with His19. The formation of this interaction may therefore represent a key step in the refolding pathway of cytochrome b_5, where a number of residues with hydrophobic side chains interact and form the second hydrophobic core *(20, 41)*. This core is preserved in the apoprotein since many of the NOE connectivities observed in holocytochrome b_5 are comparable *(23)*. As a result the faster process may represent an alternative refolding pathway, although the use of other methods for probing protein folding will confirm this possibility. The formation of the compact, low-fluorescent state of cytochrome b_5 is complete within 250 ms, but we have also noted that the heme center takes much longer to form completely (>100 s) when refolding occurs in the holoprotein (Manyusa and Whitford, 1998, unpublished results). The kinetic data support a mechanism whereby the hydrophobic core centered around Trp26 forms first and directs assembly of the heme center *(48)*. Trp26 is an invariant residue, and although a purely structural role has been envisaged, it is possible that the indole side chain forms part of a folding nucleus driving the overall process *(64)* through its specific interaction with His19 and other hydrophobic side chains. This model would predict that mutations in this region of the protein that disrupt these interactions, particularly in the transition-state complex, would inhibit the overall folding reaction, perhaps preventing assembly of the protein. Future studies will clarify this point, but the results demonstrate that refolding of cytochrome b_5 follows different pathways in the presence and absence of heme. It is perhaps not surprising in view of the complexities seen with the holoprotein that in vivo the cell appears to insert the noncovalently bound heme into a partially folded apoprotein.

SUPPORTING INFORMATION AVAILABLE

Figure 8−10, showing absorbance spectra, kinetics of protein unfolding, and dependence of refolding rates on denaturant concentration. This material is available free of charge via the Internet at http://pubs.acs.org.

REFERENCES

1. Fersht, A. R. (1993) *FEBS Lett. 325*, 5−16.
2. Jackson, S. E., and Fersht, A. R. (1991) *Biochemistry 30*, 10428−10435.
3. Matouschek, A., Kellis, J. T, Serrano, L., and Fersht, A. R. (1989) *Nature 340*, 122−126.
4. Kuwajima, K., Okayama, N., Yammamoto, K., Ishihara, T., and Sugai, S. (1991) *FEBS Lett. 290*, 135−138.
5. Walkenhorst, W. F., Green, S. M., and Roder, H. (1997) *Biochemistry 36*, 5795−5805.
6. Schindler, T., and Schmid, F. X. (1996) *Biochemistry 35*, 16833−16842.
7. Sugawara, T., Kuwajima, K., and Sugai, S. (1991) *Biochemistry 30*, 2698−2706.
8. Creighton, T. E. (1990) *Biochem. J. 270*, 1−16.
9. Fox, R. O., Evans, P. A., and Dobson, C. M. (1986) *Nature 320*, 192−194.
10. Chazin, W. J., Kordel, J., Drakenberg, T., Thulin, E., Brodin, P., Grundstrom, T., and Forsen, S. (1989) *Proc. Natl. Acad. Sci. U.S.A. 86*, 2195−2198.
11. Sauder, J. M., Mackenzie, N. E., and Roder, H. (1996) *Biochemistry 35*, 16852−16862.
12. Elove, G. A., Chaffotte, A. F., Roder, H., and Goldberg, M. E. (1992) *Biochemistry 31*, 6876−6883.
13. Smith, M. L., Paul, J., Ohlsson, P. I., Hjortsberg, K., and Paul, K. G. (1991) *Proc. Natl. Acad. Sci. U.S.A. 88*, 882−886.
14. Lederer, F. (1994) *Biochimie 76*, 674−692.
15. Strittmatter, P., and Vellick, S. F. (1956) *J. Biol. Chem. 221*, 253−264.
16. Von Bodman, S. B., Schuler, M. A., Jollie, D. R., and Sligar, S. G. (1986) *Proc. Natl. Acad. Sci. U.S.A. 83*, 9443−9447.
17. Funk, W. D., Lo, T. P., Mauk, M. R., Brayer, G. D., MacGillivray, R. T. A., and Mauk, A. G. (1990) *Biochemistry 29*, 5500−5508.
18. Hewson, R., Newbold, R. J., and Whitford, D. (1993) *Protein Eng. 6*, 953−964.
19. Newbold, R. J., Hewson, R., and Whitford, D., (1992) *FEBS Lett. 314*, 419−424.
20. Mathews, F. S., Czerwinski, E. W., and Argos, P. (1979) in *The Porphyrins* (Dolphin, D., Ed.) Vol 7, pp 107−147, Academic Press, New York.

21. Durley, R. C. E., and Mathews, F. S. (1996). *Acta Crystallogr. D52*, 65−76.
22. Muskett, F. W., Kelly, G. P., and Whitford, D. (1996) *J. Mol. Biol. 258*, 172−189.
23. Falzone, C. J., Mayer, M. R., Whiteman, E. L., Moore, C. D., and Lecomte, J. T. G. (1996) *Biochemistry 35*, 6519−6526.
24. Arnesano, F., Banci, L., Bertini, I., and Felli, I. C. (1998) *Biochemistry 37*, 173−184.
25. Mathews, F. S., Levine, M., and Argos, P. (1972) *J. Mol. Biol. 64*, 449−464.
26. McLachlan, S. J., La Mar, G. N., Burns, P. D., Smith, K. D., and Langry, K. C. (1986) *Biochim. Biophys. Acta 874*, 274−284.
27. Lee, K.-B., La Mar, G. N., Kehres, L. A., Fujinari, E. M., Smith, K. M., Pochapsky, T. C., and Sligar, S. G. (1990) *Biochemistry 29*, 9623−9631.
28. Mortuza, G. B., and Whitford, D. (1997) *FEBS Lett. 412*, 610−614.
29. Pfeil, W. (1993) *Protein Sci. 2*, 1497−1501.
30. Manyusa, S., and Whitford, D. (1999) *Biochemistry 38*, 9533−9540.
31. Barrick, D., and Baldwin, R. L. (1993) *Protein Sci. 2*, 869−876.
32. Shen, L. L., and Hermans, J. (1971) *Biochemistry 11*, 1836−1841.
33. Feng, Y., and Sligar, S. G. (1991) *Biochemistry 30*, 10150−10155.
34. Wittung-Stafshede, P., Lee, J. C., Winkler, J. R., and Gray, H. B. (1999) *Proc. Natl. Acad. Sci. U.S.A. 96*, 6587−6590.
35. Hargrove, M. S., Barrick, D., and Olson, J. S. (1996). *Biochemistry 35*, 11293−11299.
36. Hargrove, M. S., Wilkinson, A. J., and Olson, J. S. (1996) *Biochemistry 35*, 11310−11318.
37. Goto, Y., and Fink, A. L. (1994) *Methods Enzymol. 232*, 3−15.
38. Fuentes, E. J., and Wand, A. J. (1998) *Biochemistry 37*, 3687−3698.
39. Pace, C. N. (1986) *Methods Enzymol. 131*, 266−279.
40. Laidler, K. J. (1950) *Chemical Kinetics*, McGraw-Hill, New York.
41. Huntley, T. E., and Strittmatter, P. (1972) *J. Biol. Chem. 247*, 4641−4647.
42. Chen, B.-L., Baase, W. A., and Schellman, J. A. (1989) *Biochemistry 28*, 691−699.
43. Tajima, S., Enomoto, K.-I., and Sato, R. (1976) *Arch. Biochem. Biophys. 172*, 90−97.
44. Pfeil, W., and Bendzko, P. (1980) *Biochim. Biophys. Acta 626*, 73−78.
45. Yao, P., Xie, Y., Wang Y.-H., Sun, Y.-L., Huang, Z.-X., Xiao, G.-T., and Wang, S.-D. (1997) *Protein Eng. 10*, 575−581.
46. Vergeres, G., Chen, D. Y., Wu, F.-F. and Waskell, L. (1993) *Arch. Biochem. Biophys. 305*, 231−241.
47. Myers, J. K., Pace, C. N., and Scholtz, J. M. (1995) *Protein Sci. 4*, 2138−2148.
48. Pace, C. N. (1975) *CRC Crit. Rev Biochem. 3*, 1−43.
49. Moore, C. D., and Lecomte, J. T. J. (1993) *Biochemistry 32*, 199−207.
50. Grathwohl, C., and Wuthrich, K. (1981) *Biopolymers 20*, 2623−2633.
51. Brandts, J. F., Halvorson, H. R., and Brennan, M. (1975) *Biochemistry 14*, 4953.
52. Jackson, S. E., and Fersht, A. R. (1991) *Biochemistry 30*, 10436−10443.
53. Keller, R. M., and Wuthrich, K. (1980) *Biochim. Biophys. Acta, 621*, 204−217.
54. Pochapsky, T. C., Sligar, S. G., McLachlan, S. J., and La Mar, G. N. (1990) *J. Am. Chem. Soc. 112*, 5258−5263.
55. McLachlan, S. J., La Mar, G. N., Burns, P. D., Smith, K. D., and Langry, K. C. (1986) *Biochim. Biophys. Acta 874*, 274−284.
56. Hunter, C. L., Lloyd, E., Eltis, L. D., Rafferty, S. P., Lee, H., Smith, M., and Mauk, A. G. (1997) *Biochemistry 36*, 1010−1017.
57. Arnesano, F., Banci, L., Bertini, I., and Koulougliotis, D. (1998) *Biochemistry 37*, 17082−17092.
58. Dangi, B., Sarma, S., Yan, C. H., Banville, D. L., and Guiles, R. D. (1998) *Biochemistry 37*, 8289−8302.
59. Lloyd, E., Ferrer, J. C., Funk, W. D., Mauk, M. R., and Mauk, A. G. (1994) *Biochemistry 33*, 11432−11437.
60. Walker, F. A., Emrick, D., Rivera, J. E., Hanquet, B. J., and Buttlaire, D. H. (1988) *J. Am. Chem. Soc. 110*, 6234−6240.
61. Oliveberg, M. (1998) *Acc. Chem. Res. 31*, 765−772.
62. Matagne, A., Radford, S. E., and Dobson, C. M. (1997) *J. Mol. Biol. 267*, 1068−1074.
63. Robinson, C. R., Liu, Y., Thomson, J. A., Sturtevant, J. M., and Sligar, S. G. (1997) *Biochemistry 36*, 16141−16146.
64. Shakhnovich, E., Abkevich, V., and Ptitsyn, O. (1996) *Nature 379*, 96−98.
65. Koradi, R., Billeter, M. and Wuthrich, K. (1996) *J. Mol. Graphics 14*, 51−59.

BI991413J